



THE UNIVERSITY *of* EDINBURGH

Edinburgh Research Explorer

An evolutionarily conserved ribosome-rescue pathway maintains epidermal homeostasis

Citation for published version:

Liakath-Ali, K, Mills, EW, Sequeira, I, Lichtenberger, BM, Pisco, AO, Sipilä, KH, Mishra, A, Yoshikawa, H, Wu, CC-C, Ly, T, Lamond, AI, Adham, IM, Green, R & Watt, FM 2018, 'An evolutionarily conserved ribosome-rescue pathway maintains epidermal homeostasis', *Nature*, vol. 556, pp. 376–380.
<https://doi.org/10.1038/s41586-018-0032-3>

Digital Object Identifier (DOI):

[10.1038/s41586-018-0032-3](https://doi.org/10.1038/s41586-018-0032-3)

Link:

[Link to publication record in Edinburgh Research Explorer](#)

Document Version:

Peer reviewed version

Published In:

Nature

General rights

Copyright for the publications made accessible via the Edinburgh Research Explorer is retained by the author(s) and / or other copyright owners and it is a condition of accessing these publications that users recognise and abide by the legal requirements associated with these rights.

Take down policy

The University of Edinburgh has made every reasonable effort to ensure that Edinburgh Research Explorer content complies with UK legislation. If you believe that the public display of this file breaches copyright please contact openaccess@ed.ac.uk providing details, and we will remove access to the work immediately and investigate your claim.



An evolutionarily conserved ribosome-rescue pathway maintains epidermal homeostasis

Kifayathullah Liakath-Ali^{1, #}, Eric W. Mills², Inês Sequeira¹, Beate M. Lichtenberger^{1, 3}, Angela Oliveira Pisco¹, Kalle H. Sipilä¹, Ajay Mishra^{1,4}, Harunori Yoshikawa⁵, Colin Chih-Chien Wu², Tony Ly^{5,6}, Angus I Lamond⁶, Ibrahim M. Adham⁷, Rachel Green² and Fiona M. Watt¹

1. Centre for Stem Cells and Regenerative Medicine, King's College London, 28th floor, Guy's Tower Wing, London SE1 9RT, UK.
2. Howard Hughes Medical Institute, Johns Hopkins School of Medicine, Department of Molecular Biology and Genetics, Baltimore, MD 21205, USA.
3. Skin & Endothelium Research Division, Department of Dermatology, Medical University of Vienna, Lazarettgasse 14, 1090 Vienna, Austria
4. Cambridge Infinitus Research Centre, University of Cambridge, Cambridge, UK
5. Centre for Gene Regulation and Expression, School of Life Sciences, University of Dundee, Dow Street, Dundee, DD1 5EH, Scotland, UK.
6. Wellcome Trust Centre for Cell Biology, University of Edinburgh, Michael Swann Building, King's Buildings, Edinburgh EH9 3BF, Scotland, UK.
7. Institute of Human Genetics, University Medical Centre of Göttingen, D-37073 Göttingen, Germany.

Present address: Department of Molecular and Cellular Physiology and Howard Hughes Medical Institute, Stanford University Medical School, 265 Campus Drive, CA 94305-5453, USA

Address for communication: fiona.watt@kcl.ac.uk

Ribosome-associated mRNA quality control mechanisms ensure fidelity of protein translation^{1,2}. Although extensively studied in yeast, little is known about their role in mammalian tissues, despite emerging evidence that stem cell fate is controlled by translational mechanisms^{3,4}. One evolutionarily conserved component of the quality control machinery, *Dom34/Pelota (Pelo)*, rescues stalled ribosomes⁵. Here we show that *Pelo* is required for mammalian epidermal homeostasis. Conditional deletion of *Pelo* in those murine epidermal stem cells that express *Lrig1* results in hyperproliferation and abnormal differentiation. In contrast, deletion in *Lgr5*⁺ stem cells has no effect and deletion in *Lgr6*⁺ stem cells has only a mild phenotype. Loss of *Pelo* results in accumulation of short ribosome footprints and global upregulation of translation rather than affecting expression of specific genes. Translational inhibition by rapamycin-mediated down regulation of mTOR rescues the epidermal phenotype. Our study reveals a novel role for the ribosome-rescue machinery in mammalian tissue homeostasis and an unanticipated specificity in its impact on different stem cell populations.

Pelo is expressed in mouse skin dermis and epidermis⁶ (Extended Data Fig. 1a). Dermal-specific deletion (*Pelo*^{derKO}) resulted in mice that were smaller than littermate controls but had a normal lifespan and no dermal abnormalities (Fig. 1a-f). Although Dom34 forms a functional complex with Hbs1 in yeast⁷ and the mammalian homolog *Hbs1l* is expressed in mouse skin⁶ (Extended Data Fig. 1b), the *Hbs1l* knockout (from exon 5; Extended Data Fig. 1c) had no epidermal defects (Extended Data Fig. 1d-f) and only small changes in dermal collagen deposition, thickness and cell density (Extended Data Fig. 1f-m). Another *Pelo* partner, *Gtpbp2*⁸, does not have a reported skin phenotype.

Selective embryonic deletion of *Pelo* in Krt14 expressing epidermal cells, comprising the known stem cell subpopulations⁹, via *Krt14*^{Cre} (*Pelo*^{epiKO}; Fig. 1g) phenocopied deletion via the ubiquitous Rosa26 locus¹⁰. Mice were born with scaly skin and an epidermal barrier defect (increased trans epidermal water loss; TEWL). They exhibited hair and weight loss, failing to thrive beyond 5 months (Fig. 1h-k). Epidermal thickening resulted from increased proliferation (Fig. 1l-q) and abnormal accumulation of differentiated cells (Fig. 1n-t). Wound closure was delayed (Fig. 1u), correlating with reduced proliferation, differentiation and migration (Extended Data Fig. 2a-i). Hyperproliferation in unwounded skin combined with delayed wound healing and abnormal differentiation has been observed in other mouse models¹¹. There was also striking degeneration of the sebaceous glands and hair follicles, correlating with loss of the hair follicle bulge stem cell markers Krt15 and CD34 and the junctional zone stem cell marker Lrig1 (Extended Data Fig. 3a-c).

To determine whether the *Pelo* epidermal phenotype could be induced postnatally, we applied 4-OHT to adult *Pelo*^{fl/fl}; *Krt14*^{CreERT} (Extended Data Fig. 4a, b). Mice developed skin lesions, increased TEWL and delayed wound closure (Extended Data Fig. 4c-e). Degeneration of hair follicles and sebaceous glands correlated with keratinized cyst formation (Extended Data Fig. 4f, g). Sebocyte differentiation was disturbed, accompanied by expansion of Lrig1 labelling into the upper sebaceous gland (Extended Data Fig. 4h, i).

PELO knockdown in cultured human epidermal keratinocytes led to an increase in stem cell colonies (Extended Data Fig. 5a-g). Immunostaining of epidermis reconstituted on decellularised dermis revealed increased proliferation of basal layer cells and increased differentiated layers

(Extended Data Fig. 5h-l). Therefore the mouse epidermal *Pelo* phenotype was recapitulated in human cells.

To determine if there is a differential requirement for *Pelo* in different epidermal subpopulations, we conditionally deleted *Pelo* in *Lgr5*⁺, *Lgr6*⁺ and *Lrig1*⁺ stem cells (Fig. 2a-c). *Pelo* deletion in *Lrig1*⁺ cells recapitulated the effects of deleting *Pelo* in *Krt14*⁺ cells, whereas when *Pelo* was deleted in *Lgr5*⁺ and *Lgr6*⁺ cells differentiation was normal (Fig. 2d) with only a small increase in *Ki67*⁺ cells (Extended Data Fig. 5m, Fig. 2f). *Pelo* deletion in *Lrig1*⁺ cells increased cell proliferation in the upper hair follicle, with marked changes in follicles and sebaceous glands (Fig. 2e, Extended Data Fig. 6a, b). A significant increase in proliferation and TEWL occurred in the interfollicular epidermis (IFE) of *Pelo*^{fl/fl}; *Lrig1*^{CreERT2} mice compared to *Pelo*^{fl/fl}; *Lgr5*^{CreERT2} and *Pelo*^{fl/fl}; *Lgr6*^{CreERT2} mice (Extended Data Fig. 5m, Fig. 2f, h). There was a small increase in epidermal thickness in *Pelo*^{fl/fl}; *Lgr6*^{CreERT2} mice but TEWL was unaffected (Fig. 2g, h).

We next generated *Pelo*^{fl/fl}; *Lrig1*^{CreERT2}; *Rosa26*^{tdTom}, *Pelo*^{fl/fl}; *Lgr5*^{CreERT2}; *Rosa26*^{tdTom}, and *Pelo*^{fl/fl}; *Lgr6*^{CreERT2}; *Rosa26*^{tdTom} mice, and treated with 4-OHT. *Pelo* deletion did not change the contribution of *Lgr5* or *Lgr6* progeny to the epidermis (Extended Data Fig. 6c, d). In contrast, on *Pelo* deletion *Lrig1* lineage cells expanded downwards into the hair follicles and fully colonized the IFE (Extended Data Fig. 6c, d). In the presence or absence of *Pelo*, the *Lrig1* lineage accounted for most *Ki67*⁺ epidermal cells; they also accounted for the increase in proliferative cells on *Pelo* deletion (Extended Data Fig. 6e, f).

96 Yeast cells lacking *Dom34* (the homolog of *Pelo*) are enriched in short 16-18 nucleotide
97 ribosome-protected fragments (RPFs) resulting from translation to the 3' end of truncated
98 mRNAs⁵. *Dom34/Rli1* mutant yeast accumulate full length 28-32 nucleotide RPFs in 3' UTRs,
99 consistent with the role of *Dom34* and *Rli1* in ribosome rescue and recycling on intact mRNAs,
100 respectively¹². In anucleate hematopoietic cells PELO and ABCE1 (*Rli1*) rescue non-translating
101 3'UTR ribosomes¹³ and impact mRNA stability¹⁴. When we performed ribosomal profiling on
102 keratinocytes from adult *Pelo*^{epiKO} mice by deep sequencing RPFs¹⁵, RPFs mapped primarily to
103 the coding sequence (CDS) (Fig. 3a; Extended Data Fig. 7a, b), consistent with studies¹² showing
104 that loss of PELO alone does not substantially increase 3' UTR ribosomes. CDS RPFs were
105 primarily 28-34nts, the expected fragment size protected by mammalian ribosomes¹⁶, and
106 displayed the three-nucleotide periodicity reflecting codon-by-codon movement of elongating
107 ribosomes (Fig. 3b, gray bars).

108

109 *Pelo*^{epiKO} profiles were enriched in 20-21 nucleotide RPFs (~4-5% of total RPFs compared to
110 <1% in control cells) (Fig. 3a-c). Like the dominant population of 28-34nt RPFs, these footprints
111 were primarily found in the CDS and showed a strong reading frame signal, indicating they too
112 reflect the presence of elongating ribosomes, yet are shortened on their 3' end after nuclease
113 digestion (Fig. 3d, right). The density of short RPFs was evenly distributed and did not increase
114 in frequency near the downstream 3' portion of transcripts (Fig. 3a), as would be anticipated if
115 they resulted from ribosomes encountering a directional RNA decay process^{17,18}. Consistent with
116 this, enrichment for 20-21 nt footprints was not linked to reduced transcript abundance in
117 *Pelo*^{epiKO} cells (Fig. 3e; Supplementary Table 1). While *Pelo* is implicated in decay of the
118 unusual histone mRNAs that lack polyA tails¹⁹, the short footprints did not demonstrate patterns

to indicate they result from ribosomes occupying transcripts that are being degraded. The 21mer RPFs seen in *Pelo*^{epiKO} cells could be the equivalent of the 16mer species in yeast⁵ and reflect the increased size of the mammalian ribosome²⁰. However, we suggest they are equivalent to the 21nt fragments observed²¹ in anisomycin-treated yeast cells and reflect dependence on *Pelo*-associated quality control mechanisms in response to tRNA starvation in rapidly dividing cells.

Epidermal *Pelo* loss led to significant changes in global translational efficiency (TE)¹⁵ (Fig. 3f, g; $p < 0.01$). TE values for keratins and ribosomal proteins were notably increased (Fig. 3f, g). There was significant enrichment for genes involved in RNA metabolism, protein synthesis, extracellular matrix and chromatin regulation (Fig. 3h; Extended Data Fig. 7c to e; Supplementary Table 2; Supplementary Table 3). There was also differential expression of canonical translational pathways, including upregulation of the mTOR (mechanistic target of rapamycin) pathway (Fig. 3h; Extended Data Fig. 8a, b). Since mTOR signaling leads to increased global translation²² (Extended Data Fig. 8c), we compared the *Gtpbp2*/tRNA mutant⁸ and *Pelo*^{epiKO} gene expression datasets. We found significant overlap in translational signaling pathways (Extended Data Fig. 8d), suggesting that ribosome stalling is sensed by mTOR.

The polysome-to-monosome ratio was increased in *Pelo*^{epiKO} cells (Fig. 3i), suggesting an overall increase in translation or accumulation of inactive stalled ribosomes. *Krt86* transcripts were enriched in the heavy polysome fractions (Fig. 3j), consistent with the increases in TE values, suggesting increased overall translation. This was confirmed by quantifying global protein synthesis by O-propargyl-puromycin (OP-P) incorporation into newly synthesized polypeptide chains^{3,4}. OP-P incorporation was increased in *Pelo*^{epiKO} IFE and hair follicles compared to

controls. Labelling was higher in the IFE suprabasal than basal layer, consistent with increased total protein synthesis during differentiation (Fig. 4a-d)²³. The increase in OP-P labelling in total *Pelo* null keratinocytes (Fig. 4e) and stem cells (Integrin α 6-high cells; Itga6^{high}) was confirmed by flow cytometry (Extended Data Fig. 9a, Fig. 4f-j). Confocal microscopy revealed a striking increase in the size of *Pelo*^{epiKO} basal cells (Extended Data Fig. 9b-d), consistent with increased protein synthesis and a higher proportion of G2/M and S phase cells (Extended Data Fig. 9e).

In control mice, Lrig1+ cells exhibited slightly higher protein synthesis than Lgr5 and Lgr6+ cells (Fig. 4k, l). When *Pelo* was deleted, protein synthesis in Lrig1+ cells was increased further relative to Lgr5 and Lgr6+ cells (Fig. 4k, l). RNA-seq (Extended Data Fig. 10a) revealed that regardless of whether or not *Pelo* was expressed, Lgr5+ cells clustered separately from Lrig1+ and Lgr6+ cells, while the gene expression profiles of individual populations did not cluster based on *Pelo* expression (Extended Data Fig. 10b-j, Supplementary Tables 4, 5). Therefore the *Pelo* epidermal phenotype primarily reflects increased translation, rather than expression of specific genes.

To down regulate mTOR1²², we applied rapamycin to adult *Pelo*^{epiKO} skin (Extended Data Fig. 9f, g). There was a significant reduction in Ki67+ cells compared to controls (Extended Data Fig. 9h-j). Phosphorylated ribosomal protein S6K (pS6K), a key substrate of mTOR²², was increased in *Pelo*^{epiKO} skin, and reduced by rapamycin (Extended Data Fig. 9k). However, rapamycin did not prevent disruption of hair follicle and sebaceous gland architecture (Extended Data Fig. 9h).

Simultaneous rapamycin treatment and *Pelo* deletion largely prevented *Pelo*-mediated disruption of epidermal homeostasis (Fig. 4m, n). TEWL, epidermal thickening and proliferation were substantially reduced (Fig. 4o-u; Extended Data Fig. 9l); pS6K labeling was reduced (Fig. 4v) and phosphorylation of another mTOR substrate, 4EBP1, was decreased (Extended Data Fig. 9m). Therefore the epidermal *Pelo* deletion phenotype is largely attributable to increased protein translation.

Our results indicate that translational control is critical for tissue homeostasis^{3,4,13} and establish a link between *Pelo* inactivation and translational activation via mTOR. mTOR is known to regulate cell growth and proliferation^{22,24} and is activated upon ribosome-stalling by Fragile X Mental Retardation Protein^{25,26}. Impaired ribosomal biogenesis also activates mTOR1 signaling and stimulates translation initiation and elongation factors²⁷. mTOR signaling may be activated to enhance the efficiency of the translational machinery in order to compensate for impaired or reduced availability of ribosomes^{8,28}.

The increased size of *Pelo*-null epidermal cells as a result of increased protein synthesis^{23,30} may stimulate differentiation through decreased basement membrane engagement²⁹ and thus indirectly promote proliferation. Factors that may account for the selective sensitivity of Lrig1+ cells to *Pelo* deletion, include their proliferative state, abundance and location relative to Lgr5+ and Lgr6+ cells, together with their known ability to repopulate different epidermal compartments³¹.

Acknowledgements

We dedicate this work to Wolfgang Engel. FMW gratefully acknowledges funding from the Wellcome Trust and UK Medical Research Council. We are also grateful for funding from the Department of Health via the National Institute for Health Research comprehensive Biomedical Research Centre award to Guy's & St Thomas' National Health Service Foundation Trust in partnership with King's College London and King's College Hospital NHS Foundation Trust. RG acknowledges funding from Howard Hughes Medical Institute. We thank Dr. Christopher Lelliott and Valerie Vancollie for providing *Hbs1l* knockout samples, Drs. Benedicte Oules for critical reading of the manuscript, Drs. D. V. Krishna Pantakani, Aamir Ahmed, Shukry Habib, Ignacio Sancho-Martinez, Giacomo Donati, Magnus Lynch and all Wattlab members for helpful discussions. Technical help from Mr. Chaozheng Li, Mr. Matteo Battilocchi and staff at the Nikon Imaging Centre and the Hodgkin Biological Services Facility, King's College London is gratefully acknowledged. We thank the High-Throughput Genomics Group at the Wellcome Trust Centre for Human Genetics (funded by Wellcome Trust: 203141/Z/16/Z) for generation of the sequencing data.

Author contributions

KL and FMW conceptualized the study. KL, IS and BML performed and analysed mouse experiments. KHS and AJ performed and analysed cell culture experiments. AOP analysed data from ribosome profile and RNA-seq experiments. IMA generated the *Pelo* conditional knockout mouse. EWM, CCW and RG generated and analysed ribosome-profiling data. HY, TL and AIL generated and analyzed polysome data. KL and FMW wrote the manuscript with input from all authors.

Author Information

Authors declare no competing financial interests. Correspondence and requests should be addressed to Fiona Watt (Fiona.watt@kcl.ac.uk).

References

- 1 Brandman, O. & Hegde, R. S. Ribosome-associated protein quality control. *Nat Struct Mol Biol* **23**, 7-15, doi:10.1038/nsmb.3147 (2016).
- 2 Shoemaker, C. J. & Green, R. Translation drives mRNA quality control. *Nat Struct Mol Biol* **19**, 594-601, doi:10.1038/nsmb.2301 (2012).
- 3 Blanco, S. *et al.* Stem cell function and stress response are controlled by protein synthesis. *Nature* **534**, 335-340, doi:10.1038/nature18282 (2016).
- 4 Signer, R. A., Magee, J. A., Salic, A. & Morrison, S. J. Haematopoietic stem cells require a highly regulated protein synthesis rate. *Nature* **509**, 49-54, doi:10.1038/nature13035 (2014).
- 5 Guydosh, N. R. & Green, R. Dom34 rescues ribosomes in 3' untranslated regions. *Cell* **156**, 950-962, doi:10.1016/j.cell.2014.02.006 (2014).
- 6 Rezza, A. *et al.* Signaling Networks among Stem Cell Precursors, Transit-Amplifying Progenitors, and their Niche in Developing Hair Follicles. *Cell Rep* **14**, 3001-3018, doi:10.1016/j.celrep.2016.02.078 (2016).
- 7 Becker, T. *et al.* Structure of the no-go mRNA decay complex Dom34-Hbs1 bound to a stalled 80S ribosome. *Nat Struct Mol Biol* **18**, 715-720, doi:10.1038/nsmb.2057 (2011).
- 8 Ishimura, R. *et al.* RNA function. Ribosome stalling induced by mutation of a CNS-specific tRNA causes neurodegeneration. *Science* **345**, 455-459, doi:10.1126/science.1249749 (2014).
- 9 Kretzschmar, K., Weber, C., Driskell, R. R., Calonje, E. & Watt, F. M. Compartmentalized Epidermal Activation of beta-Catenin Differentially Affects Lineage Reprogramming and Underlies Tumor Heterogeneity. *Cell Rep* **14**, 269-281, doi:10.1016/j.celrep.2015.12.041 (2016).
- 10 Elkenani, M. *et al.* Pelota Regulates Epidermal Differentiation by Modulating BMP and PI3K/AKT Signaling Pathways. *J Invest Dermatol* **136**, 1664-1671, doi:10.1016/j.jid.2016.04.020 (2016).
- 11 Florin, L. *et al.* Delayed wound healing and epidermal hyperproliferation in mice lacking JunB in the skin. *J Invest Dermatol* **126**, 902-911, doi:10.1038/sj.jid.5700123 (2006).
- 12 Young, D. J., Guydosh, N. R., Zhang, F., Hinnebusch, A. G. & Green, R. Rli1/ABCE1 Recycles Terminating Ribosomes and Controls Translation Reinitiation in 3'UTRs In Vivo. *Cell* **162**, 872-884, doi:10.1016/j.cell.2015.07.041 (2015).
- 13 Mills, E. W., Wangen, J., Green, R. & Ingolia, N. T. Dynamic Regulation of a Ribosome Rescue Pathway in Erythroid Cells and Platelets. *Cell Rep* **17**, 1-10, doi:10.1016/j.celrep.2016.08.088 (2016).
- 14 Mills, E. W., Green, R. & Ingolia, N. T. Slowed decay of mRNAs enhances platelet specific translation. *Blood* **129**, e38-e48, doi:10.1182/blood-2016-08-736108 (2017).

- 15 Ingolia, N. T., Brar, G. A., Rouskin, S., McGeachy, A. M. & Weissman, J. S. The ribosome profiling strategy for monitoring translation in vivo by deep sequencing of ribosome-protected mRNA fragments. *Nat Protoc* **7**, 1534-1550, doi:10.1038/nprot.2012.086 (2012).
- 16 Ingolia, N. T., Lareau, L. F. & Weissman, J. S. Ribosome profiling of mouse embryonic stem cells reveals the complexity and dynamics of mammalian proteomes. *Cell* **147**, 789-802, doi:10.1016/j.cell.2011.10.002 (2011).
- 17 Gydosh, N. R., Kimmig, P., Walter, P. & Green, R. Regulated Ire1-dependent mRNA decay requires no-go mRNA degradation to maintain endoplasmic reticulum homeostasis in *S. pombe*. *Elife* **6**, doi:10.7554/eLife.29216 (2017).
- 18 Gydosh, N. R. & Green, R. Translation of poly(A) tails leads to precise mRNA cleavage. *RNA* **23**, 749-761, doi:10.1261/rna.060418.116 (2017).
- 19 Slevin, M. K. *et al.* Deep sequencing shows multiple oligouridylations are required for 3' to 5' degradation of histone mRNAs on polyribosomes. *Mol Cell* **53**, 1020-1030, doi:10.1016/j.molcel.2014.02.027 (2014).
- 20 Ben-Shem, A., Jenner, L., Yusupova, G. & Yusupov, M. Crystal structure of the eukaryotic ribosome. *Science* **330**, 1203-1209, doi:10.1126/science.1194294 (2010).
- 21 Lareau, L. F., Hite, D. H., Hogan, G. J. & Brown, P. O. Distinct stages of the translation elongation cycle revealed by sequencing ribosome-protected mRNA fragments. *Elife* **3**, e01257, doi:10.7554/eLife.01257 (2014).
- 22 Thoreen, C. C. *et al.* A unifying model for mTORC1-mediated regulation of mRNA translation. *Nature* **485**, 109-113, doi:10.1038/nature11083 (2012).
- 23 Kristensen, A. R., Gsponer, J. & Foster, L. J. Protein synthesis rate is the predominant regulator of protein expression during differentiation. *Mol Syst Biol* **9**, 689, doi:10.1038/msb.2013.47 (2013).
- 24 Laplante, M. & Sabatini, D. M. mTOR signaling in growth control and disease. *Cell* **149**, 274-293, doi:10.1016/j.cell.2012.03.017 (2012).
- 25 Darnell, J. C. *et al.* FMRP stalls ribosomal translocation on mRNAs linked to synaptic function and autism. *Cell* **146**, 247-261, doi:10.1016/j.cell.2011.06.013 (2011).
- 26 Sawicka, K., Pyronneau, A., Chao, M., Bennett, M. V. & Zukin, R. S. Elevated ERK/p90 ribosomal S6 kinase activity underlies audiogenic seizure susceptibility in fragile X mice. *Proc Natl Acad Sci U S A* **113**, E6290-E6297, doi:10.1073/pnas.1610812113 (2016).
- 27 Liu, R. *et al.* Impairing the production of ribosomal RNA activates mammalian target of rapamycin complex 1 signalling and downstream translation factors. *Nucleic Acids Res* **42**, 5083-5096, doi:10.1093/nar/gku130 (2014).
- 28 Mills, E. W. & Green, R. Ribosomopathies: There's strength in numbers. *Science* **358**, doi:10.1126/science.aan2755 (2017).
- 29 Watt, F. M., Jordan, P. W. & O'Neill, C. H. Cell shape controls terminal differentiation of human epidermal keratinocytes. *Proc Natl Acad Sci U S A* **85**, 5576-5580 (1988).
- 30 Gingold, H. *et al.* A dual program for translation regulation in cellular proliferation and differentiation. *Cell* **158**, 1281-1292, doi:10.1016/j.cell.2014.08.011 (2014).
- 31 Page, M. E., Lombard, P., Ng, F., Gottgens, B. & Jensen, K. B. The epidermis comprises autonomous compartments maintained by distinct stem cell populations. *Cell Stem Cell* **13**, 471-482, doi:10.1016/j.stem.2013.07.010 (2013).

Methods

Mouse strains

All mouse experiments were performed under a UK Government Home Office project license and subject to local institutional ethical approval. The generation of conditional *Pelo*^{fl/fl} (*Pelo*^{tm1Imad}) mice was described elsewhere³². To derive constitutive *Pelo* epidermal knockout mice (*Pelo*^{epiKO}), *Pelo*^{fl/fl} mice were crossed with *Krt14*^{Cre} mice (Jax strain, stock number 004782). To achieve temporally controlled *Pelo* knockout and genetic labeling of cells lacking *Pelo*, *Pelo*^{fl/fl} mice were crossed with *Krt14*^{CreERT} (Jax strain, stock number 005107), *Lrig1*^{EGFP-IRES-CreERT2} mice³¹, *Lgr5*^{EGFP-IRES-CreERT2} mice³³, *Lgr6*^{EGFP-IRES-CreERT2} mice³⁴ and *Rosa26*^{LoxP-Stop-LoxP-tdTomato} mice³⁵. To activate Cre recombinase, 4-Hydroxytamoxifen (4-OHT, Sigma-Aldrich) was dissolved in acetone and applied topically (3 mg/100 µl) every day for five days and once a week for three weeks. For proliferation assays, 5-ethynyl-2'-deoxyuridine (EdU) (Invitrogen, 20 mg kg⁻¹ body mass; in PBS) was injected intraperitoneally and the tissue was harvested 1 hr later. To derive constitutive *Pelo* dermal knockout mice (*Pelo*^{derKO}), *Pelo*^{fl/fl} mice were crossed with *Dermo1*^{Cre} (B6.129X1-*Twist2*^{tm1.1(cre)Dor/J})^{36,37}. Mouse lines used in this study with the location of expression of markers in the skin are illustrated in the Extended Data Fig. 10k. *Hbs1l*^{-/-} (*Hbs1l*^{tm1a(KOMP)Wtsi}) mice were produced at the Wellcome Trust Sanger Institute Mouse Genetics Project as part of International Mouse Phenotype Consortium (IMPC)³⁸.

Library generation for ribosome profiling

Samples of *Pelo*^{epiKO} epidermis for ribosome profiling and RNA-Seq were prepared by scrapping off the epidermal layer in liquid nitrogen. Frozen samples were ground using a Mixer Mill (Retch) and thawed in the presence of polysome lysis buffer. Lysates were clarified by

centrifugation at 20,000g for 10 minutes at 4°C and the supernatant was collected. Total lysate RNA was quantified using the Quant-it RNA kit (Thermo) and 5 µg was used for preparation of ribosome profiling libraries as described previously¹⁵. Total RNA was size-selected by excising gel regions between phosphorylated 16nt and 34nt RNA oligo standards. Ribosomal RNAs were depleted using Ribo-Zero Gold (Illumina) after footprint size-selection. 100ng was used for preparation of RNA-Sequencing libraries from the same samples as profiling libraries. Analysis using a BioAnalyzer total RNA pico chip was used to confirm RNA integrity (RIN >9) for RNA sequencing samples. The datasets are deposited in GEO under accession number GSE94385.

Sequencing and data analysis

Ribosome profiling and RNA-Seq libraries were sequenced using a HiSeq2500 (Illumina). ~110 million total raw reads were generated from 4 ribosome profiling samples with between 11 and 30 million reads mapping to the genome per sample. For ribosome profiling analysis, only singly-mapped reads (NH:i:1) with no mismatches (NM:I:0) were used. Translational efficiency (TE) was calculated as number of CDS RPFs / RPKM. Relative 3'UTR ribosome occupancy was calculated as 3'UTR footprint density / CDS footprint density. For differential gene expression analysis, we uploaded the list of differentially expressed genes into Ingenuity IPA and ran a core analysis. This identified the top molecules, pathways and master regulators that are different between control and *Pelo*^{epiKO} samples.

Polysome analysis

Epidermal layers from WT and *Pelo*^{epiKO} were lysed as described above (see Library generation for ribosome profiling). Clarified lysates were loaded on 10-50% sucrose gradients prepared in polysome gradient buffer (20mM Tris-HCl [pH8], 150mM KCl, 5mM MgCl₂, 0.5mM DTT,

0.1mg/mL cycloheximide), and gradients were spun in an SW41-Ti rotor at 40,000 rpm for 3 hr at 4°C. Gradients were fractionated using a Brandel Density Gradient Fractionation System. Prior to RNA extraction, CLuc mRNA (NEB) was added in each fraction. RNA was extracted using hot acidic phenol and cDNA was synthesized using iScript cDNA synthesis kit (Bio-Rad) according to manufacturer's instructions. qPCR was carried out using iTaq Universal SYBR Green Supermix (Bio-Rad). Relative mRNA abundances in indicated fractions were normalized to CLuc mRNA to account for differences in RNA extraction efficiency among fractions, and then calculated as fold changes normalized to 80S fractions. qPCR primers: CLuc Forward 5'-GCTTCAACATCACCGTCATTG-3', CLuc Reverse 5'-CACAGAGGCCAGAGATCATTC-3', Krt86 Forward 5'-AACAGAATGATCCAGAGGCTG-3', Krt86 Reverse 5'-GCTCAGATTGGGTCACGG-3'.

RNA-seq library preparation and analysis

Primary epidermal cell suspension was prepared as previously described³⁹. Briefly, cells were harvested from 3 months old 4-OHT treated *Pelo*^{fl/+}; *Lrig1*^{EGFP-CreERT2}, *Pelo*^{fl/+}; *Lgr5*^{EGFP-CreERT2}, *Pelo*^{fl/+}; *Lgr6*^{EGFP-CreERT2} control mice and *Pelo*^{fl/fl}; *Lrig1*^{EGFP-CreERT2}, *Pelo*^{fl/fl}; *Lgr5*^{EGFP-CreERT2}, *Pelo*^{fl/fl}; *Lgr6*^{EGFP-CreERT2} *Pelo* mut mice. Total epidermal population was FACS sorted for GFP+ cells on a BD FACS Aria II cell Sorter and 1000 GFP-high cells collected from each population for RNA-seq. Library construction and the strategy for RNA-seq was performed using Smart-seq2 method as reported previously⁴⁰. Fastq files of paired-end reads were uploaded to Galaxy platform⁴¹ and aligned using STAR aligner⁴² to *Mus musculus* reference genome (GRCm38/Mm10). BAM files were processed in R using "rnaSeqGene" workflow⁴³. The data were analysed using the edgeR package. Processed data were mined using IPA Ingenuity

Pathway Analysis (Qiagen). The datasets are deposited in GEO under accession number GSE106246.

Flow cytometry for measurement of cell size, cycle and protein synthesis *in vivo*

To analyse cell size by flow cytometry, epidermal cells were isolated as previously described³⁹. Briefly, epidermis was enzymatically separated from dermis with thermolysin (Sigma, 0.25 mg/mL in PBS) overnight at 4°C. Epidermal sheets were processed into single cell suspensions by incubation in DMEM (Gibco) containing DNase (Sigma, 250 µg/mL) for 20 min at 37°C with shaking. Single cells were labelled according to standard procedures with anti- Integrin α6-Alexa Fluor 647 or FITC (AbSource, 1:20) antibody. To assess the percentage of proliferating epidermal cells, mice were injected with 500µg 5-ethynyl-2'-deoxyuridine (EdU; 2.5mg/mL in PBS) intraperitoneally and back skin was harvested 2 hr later. Cells were isolated as described above and single cell suspensions were stained with the Click-iT EdU Alexa Fluor 488 Flow Cytometry Kit (Invitrogen) according to the manufacturer's suggestions. Cell cycle analysis was performed on a BD LSR Fortessa cell analyser. Proliferating cells that had incorporated EdU were detected in the FITC/Alexa Fluor 488 channel.

To measure protein synthesis *in vivo*, mice received an intraperitoneal injection of O-propargyl-puromycin (OP-P) (Medchem Source or Thermo Fisher (C10459); 50 mg kg⁻¹ body mass; pH 6.4–6.6 in PBS). One hour later mice were euthanized and back and tail skin samples were collected. Epidermal dissociation was performed as described above. The staining for detection of protein synthesis was performed according to the manufacturer instructions (Click-iT Plus OPP Protein Synthesis Assay Kit; Thermofisher Scientific). Samples from PBS-injected mice were also stained for detection of protein synthesis and the fluorescence signal was used to

determine background labelling. Rates of protein synthesis were calculated as described previously³. Briefly, OP-P signals were normalized to whole epidermis after subtracting autofluorescence background. 'Mean OP-Puro fluorescence' reflected fluorescence values for each cell population normalized to whole epidermis. Labelled cells were analysed on a BD LSRFortessa cell analyser. All data were analysed using FlowJo software.

Histology, epidermal wholemounts and imaging

For paraffin sections, skin samples were fixed with 10% neutral buffered formalin overnight before paraffin embedding. The tissues were sectioned and stained with haematoxylin and eosin (H&E) and Herovici's stain by conventional methods. For frozen sections, skin samples were embedded on OCT (optimal cutting temperature compound; VWR), sectioned and fixed in 4% PFA for 10 min before staining. Slides were mounted using ProLong Gold anti-fade reagent containing DAPI (Life Technologies) as a nuclear counterstain. Images were acquired using a Hamamatsu slide scanner and analysed using NanoZoomer software (Hamamatsu).

The epidermal wholemount labelling procedure was performed as described previously^{44,45}. In brief, mouse tail was slit on the ventral side lengthways. Pieces (0.5x0.5 cm²) of skin were incubated in 5 mM EDTA in PBS at 37 °C for 4 h. Epidermis was gently peeled from dermis as an intact sheet in a proximal to distal direction, corresponding to the orientation of the hairs, and then the epidermis was fixed in 4% paraformaldehyde (PFA; Sigma) for 1 h at room temperature. Fixed epidermal sheets were washed in PBS and stored in PBS containing 0.2% sodium azide at 4° C.

Confocal image acquisition of stained wholemounts and skin sections were performed using a

Nikon A1 confocal microscope. Images were analysed using NIS Elements (Nikon Instruments Inc.). Photoshop CS5 (Adobe image suite) was used to optimize the images globally for brightness, contrast and colour balance.

Rapamycin treatment

Rapamycin (LC Laboratories, R5000) was dissolved in acetone. Rapamycin treatment groups received topical applications of 500 μ l 0.2% Rapamycin on dorsal and tail skin. Vehicle treatment group mice received an equal volume of acetone without rapamycin. Dorsal skin was shaved before the day of treatment.

Wound and TEWL assays

Full-thickness wounds were made on the lower dorsal skin (5mm) or tail (2mm) using punch biopsy (Stiefel) under analgesia and general anaesthesia. The hair on the back was shaved prior to wounding. Wound closure was measured using a Vernier scale. Epidermal barrier function was assessed by testing basal transepidermal water loss (TEWL) on the dorsal skin of mice using a TEWAmeter (Courage and Khazaka, TM210). Measurements were collected for 15–20 seconds when TEWL readings had stabilized, at approximately 30 seconds after the probe collar was placed on the dorsal skin.

Antibodies

Primary antibodies for wholemount and tissue sections were: chicken anti-Krt14 (Covance, SIG2376, 1:500) or directly conjugated (AlexaFluor 555) Krt14 (LL002, in house, 1:200); directly conjugated (AlexaFluor 488) Krt15 (LHK-15, in-house, 1:50); human anti-p63 (SCBT, sc367333, 1:100); rabbit anti-filaggrin (Covance, PRB-417P, 1:100); mouse anti-FASN (SCBT,

sc48357, 1:100); rabbit anti-Ki67 (Novocastra, NCL-Ki67p, 1:500); rabbit anti-Ki67 (abcam, ab16667, 1:500); rabbit anti- Phospho-S6 Ribosomal Protein (Ser235/236) (pS6K, Cell signaling, 2211, 1:200); rabbit anti-P-Cadherin (Cell signaling, 2130, 1:200); rabbit anti-Vimentin (Cell signaling, 5741s, 1:500); rabbit anti-K10 (Covance, PRB-159P, 1:500); FITC conjugated rat anti-CD49f (Integrin α 6, Biolegend, 313606, 1:100); goat anti-Lrig1 (R&D Systems, FAB3688G, 1:200); rabbit anti-Scd1 (Cell signaling, 2794s, 1:500); mouse anti-involucrin (SY5, in-house, 1:500); mouse anti-Pankeratin (abcam, ab8068, 1:200); rat anti-CD34 (RAM34, Thermo Fisher, 14-0341-82, 1:200); Rabbit anti-Phospho-4EBP1 (Thr37/46) (Cell Signalling, 236B4, 1:500) AlexaFluor (Life Technologies) dye-conjugated secondary antibodies were used at 1:250 dilutions.

***In vitro* knockdown, clonogenicity and skin reconstitution assay**

Primary human keratinocytes (strain km) were isolated from neonatal foreskin and cultured on mitotically inactivated 3T3-J2 feeder cells in complete FAD medium, containing 1 part Ham's F12 medium and three parts Dulbecco's modified Eagle's medium (DMEM), 10⁻⁴ M adenine, 10% (v/v) FBS, 0.5 μ g ml⁻¹ hydrocortisone, 5 μ g ml⁻¹ insulin, 10⁻¹ M cholera toxin and 10 ng ml⁻¹ EGF, as described previously^{46,47}. siRNA mediated gene silencing was performed as described previously⁴⁸. Briefly, keratinocytes were transferred to feeder free conditions in keratinocyte serum-free medium (KSFM) containing 30 μ g ml⁻¹ BPE (bovine pituitary extract) and 0.2 ng ml⁻¹ EGF (Gibco) for 2–3 days. Cells were trypsinized at ~70% confluence and resuspended in cell line buffer SF (Lonza). For each 20 μ l transfection (program FF-113), 2 \times 10⁵ cells were mixed with 1–2 μ M siRNA duplexes (Silencer select siRNA for *PELO* ID131910, ID131911, ID131912, as well as negative control, Ambion). Transfected cells were incubated at

room temperature for 5–10 min and subsequently resuspended in pre-warmed KSFM. siRNA nucleofections were performed with the Amaxa 16-well shuttle system (Lonza). Alternatively, keratinocytes cells were transfected by using INTERFERin (Polyplus transfections): 36pmol siRNA, 4ul INTERFERin reagent, and 200ul KSFM were mixed in the collagen coated (20ug/ml in PBS, 1h, 37°) 12-well plate and incubated 20min at room temperature. After the incubation, 75, 000 keratinocytes were seeded to the well (final concentration of siRNA 30nM). Medium was changed after 4 hrs and cells were harvested after 48 hrs.

For clonogenicity assays, nucleofected keratinocytes were seeded at low density (100-250 cells per well) on a prepared feeder layer in 6-well plates containing FAD medium. Keratinocytes were maintained in culture for 12 days and then feeders were removed by Versene treatment combined with tapping the culture flask. Once all the feeder cells were washed away, the remaining keratinocytes colonies were fixed with 4% PFA at room temperature for 10 min. Colonies were then stained with 1% Rhodanile Blue (1:1 mixture of Rhodamine B and Nile Blue A (Acros Organics) solution for 15min and washed with distilled water prior to examination. Stained dishes containing keratinocyte colonies were imaged using a Molecular Imager Gel Doc XR+ imaging system (Bio-Rad). Colonies were measured using ImageJ and clonogenicity was calculated as the percentage of plated cells that formed colonies.

For the skin reconstitution assay, pre-confluent keratinocyte cultures (KM passage 3) were disaggregated and transfected either with *PELO* siRNAs or scrambled control siRNAs. 24 hours post-transfection, keratinocytes were collected and reseeded on irradiated de-epidermised human dermis in 6-well Transwell plates with feeders and cultured at the air–liquid interface for three

weeks⁴⁹. Organotypic cultures were fixed in 10% neutral buffered formalin (overnight), paraffin embedded and sectioned for H&E and immunofluorescence analysis.

Picrosirius birefringence and dermal thickness and cell density

12µm paraffin sections were stained with picrosirius red using a standard method⁵⁰. Briefly, the sections were de-paraffinized, washed twice with water and stained 1 hr in picrosirius red solution (0.1% Sirius red F3B in saturated aqueous solution of picric acid). After the staining, sections were washed twice with acidified water (0.5 % acetic acid), dehydrated, cleared with xylene, and mounted with DPX mounting medium. The images were acquired using Zeiss Axiophot microscope and AxioCam HRc camera under plane-polarized light. The quantification of total collagen fibers was performed by Fiji (ImageJ) software. The collagen pixels were selected by Color Treshold tool (Hue 0-100, Saturation 0-255 and Brightness 230-255). Thickness of dermis was quantified by NanoZoomer Digital Pathology software (Hamamatsu). The number of cells was determined with ImageJ by counting the nucleus in DAPI stained tissue sections.

Statistics

Statistical significance in all experiments was calculated by Student's *t* test. Data are represented as mean ±SEM (error bars). GraphPad Prism was used for calculation and illustration of graphs.

Data Availability

All experimental data generated during/and or analysed this study are included in this published article (and its supplementary information files). In addition, ribosome profiling data (accession number GSE94385) and RNAseq data (accession number GSE106246) are available in GEO.

References cited in Methods

- 32 Nyamsuren, G. *et al.* Pelota regulates the development of extraembryonic endoderm through activation of bone morphogenetic protein (BMP) signaling. *Stem Cell Res* **13**, 61-74, doi:10.1016/j.scr.2014.04.011 (2014).
- 33 Barker, N. *et al.* Identification of stem cells in small intestine and colon by marker gene Lgr5. *Nature* **449**, 1003-1007, doi:10.1038/nature06196 (2007).
- 34 Snippert, H. J. *et al.* Lgr6 marks stem cells in the hair follicle that generate all cell lineages of the skin. *Science* **327**, 1385-1389, doi:10.1126/science.1184733 (2010).
- 35 Madisen, L. *et al.* A robust and high-throughput Cre reporting and characterization system for the whole mouse brain. *Nat Neurosci* **13**, 133-140, doi:10.1038/nn.2467 (2010).
- 36 Sosis, D., Richardson, J. A., Yu, K., Ornitz, D. M. & Olson, E. N. Twist regulates cytokine gene expression through a negative feedback loop that represses NF-kappaB activity. *Cell* **112**, 169-180 (2003).
- 37 Lichtenberger, B. M., Mastrogiannaki, M. & Watt, F. M. Epidermal beta-catenin activation remodels the dermis via paracrine signalling to distinct fibroblast lineages. *Nat Commun* **7**, 10537, doi:10.1038/ncomms10537 (2016).
- 38 Skarnes, W. C. *et al.* A conditional knockout resource for the genome-wide study of mouse gene function. *Nature* **474**, 337-342, doi:10.1038/nature10163 (2011).
- 39 Jensen, K. B., Driskell, R. R. & Watt, F. M. Assaying proliferation and differentiation capacity of stem cells using disaggregated adult mouse epidermis. *Nat Protoc* **5**, 898-911, doi:10.1038/nprot.2010.39 (2010).
- 40 Picelli, S. *et al.* Full-length RNA-seq from single cells using Smart-seq2. *Nat Protoc* **9**, 171-181, doi:10.1038/nprot.2014.006 (2014).
- 41 Afgan, E. *et al.* The Galaxy platform for accessible, reproducible and collaborative biomedical analyses: 2016 update. *Nucleic Acids Res* **44**, W3-W10, doi:10.1093/nar/gkw343 (2016).
- 42 Dobin, A. *et al.* STAR: ultrafast universal RNA-seq aligner. *Bioinformatics* **29**, 15-21, doi:10.1093/bioinformatics/bts635 (2013).
- 43 Love, M. I., Anders, S., Kim, V. & Huber, W. RNA-Seq workflow: gene-level exploratory analysis and differential expression. *F1000Res* **4**, 1070, doi:10.12688/f1000research.7035.1 (2015).
- 44 Braun, K. M. *et al.* Manipulation of stem cell proliferation and lineage commitment: visualisation of label-retaining cells in wholemounts of mouse epidermis. *Development* **130**, 5241-5255, doi:10.1242/dev.00703 (2003).
- 45 Liakath-Ali, K. *et al.* Novel skin phenotypes revealed by a genome-wide mouse reverse genetic screen. *Nat Commun* **5**, 3540, doi:10.1038/ncomms4540 (2014).
- 46 Lowell, S., Jones, P., Le Roux, I., Dunne, J. & Watt, F. M. Stimulation of human epidermal differentiation by delta-notch signalling at the boundaries of stem-cell clusters. *Curr Biol* **10**, 491-500 (2000).
- 47 Gandarillas, A. & Watt, F. M. Changes in expression of members of the fos and jun families and myc network during terminal differentiation of human keratinocytes. *Oncogene* **11**, 1403-1407 (1995).
- 48 Mulder, K. W. *et al.* Diverse epigenetic strategies interact to control epidermal differentiation. *Nat Cell Biol* **14**, 753-763, doi:10.1038/ncb2520 (2012).

- 49 Sen, G. L., Reuter, J. A., Webster, D. E., Zhu, L. & Khavari, P. A. DNMT1 maintains
progenitor function in self-renewing somatic tissue. *Nature* **463**, 563-567,
doi:10.1038/nature08683 (2010).
50 Lattouf, R. *et al.* Picrosirius red staining: a useful tool to appraise collagen networks in
normal and pathological tissues. *J Histochem Cytochem* **62**, 751-758,
doi:10.1369/0022155414545787 (2014).

Supplementary Tables

Table S1: List of specific keratins enriched for short footprints

Table S2: GO analysis of transcripts enriched in short ribosomal footprints. Genes enriched for
each GO category are presented in separate tabs.

Table S3: GO analysis of differentially expressed transcripts. Genes enriched for each GO
category are presented in separate tabs.

Table S4: List of differentially expressed genes among Lrig1+, Lgr5+, Lgr6+ control and Pello-
mutant populations, intersections between Lrig1+, Lgr5+, Lgr6+ control and Pello-mutant
populations.

Table S5: List of upstream regulators and canonical pathways activated in among and between
control Lrig1+, Lgr5+ and Lgr6+ subpopulations.

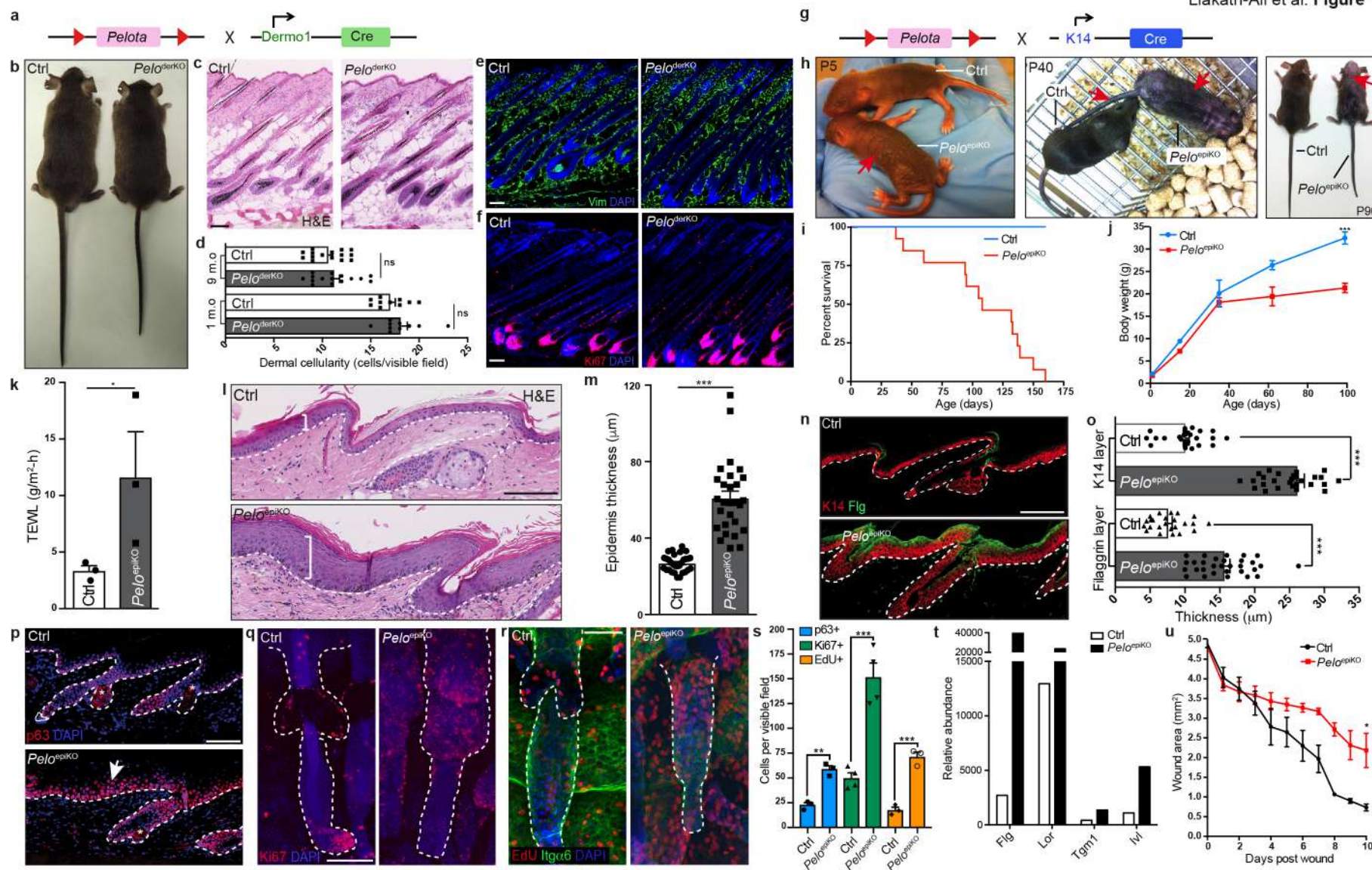


Fig. 1. Differential effects of *Pelo* deletion *Pelo*^{derKO} (a-f) and *Pelo*^{epiKO} (g-u) mice. (h) Arrows: skin abnormalities. (c, d, l, m) H&E staining of back (c, d) and tail (l, m) skin. Dermal cellularity (d) and epidermal thickness (m) were measured. n=2-4 sections from n=3 mice. (e, f, n, p-r) Immunolabelling of sections (e, f, n, p) and wholemounts (q, r). Asterisks: non-specific; arrow: suprabasal labelling; dashed lines: epidermal-dermal boundary. (m, n) *** $p < 0.001$, n=3 mice. (i) Kaplan-Meier curves (n=29 mice). (j) Body weight: *** $p < 0.0003$; n=5 per group. (k) TEWL. $p < 0.05$; n=3. (s) Quantification of proliferation. ** $p = 0.0086$; *** $p = 0.0003$ for Ki67; 0.0006 for EdU; n=3. (t) Cumulative mean values of gene expression from ribosome profiling. (u) Wound closure. * $p = 0.0500$; n=3. Ctrl: littermate controls. Scale bars 100 μm .

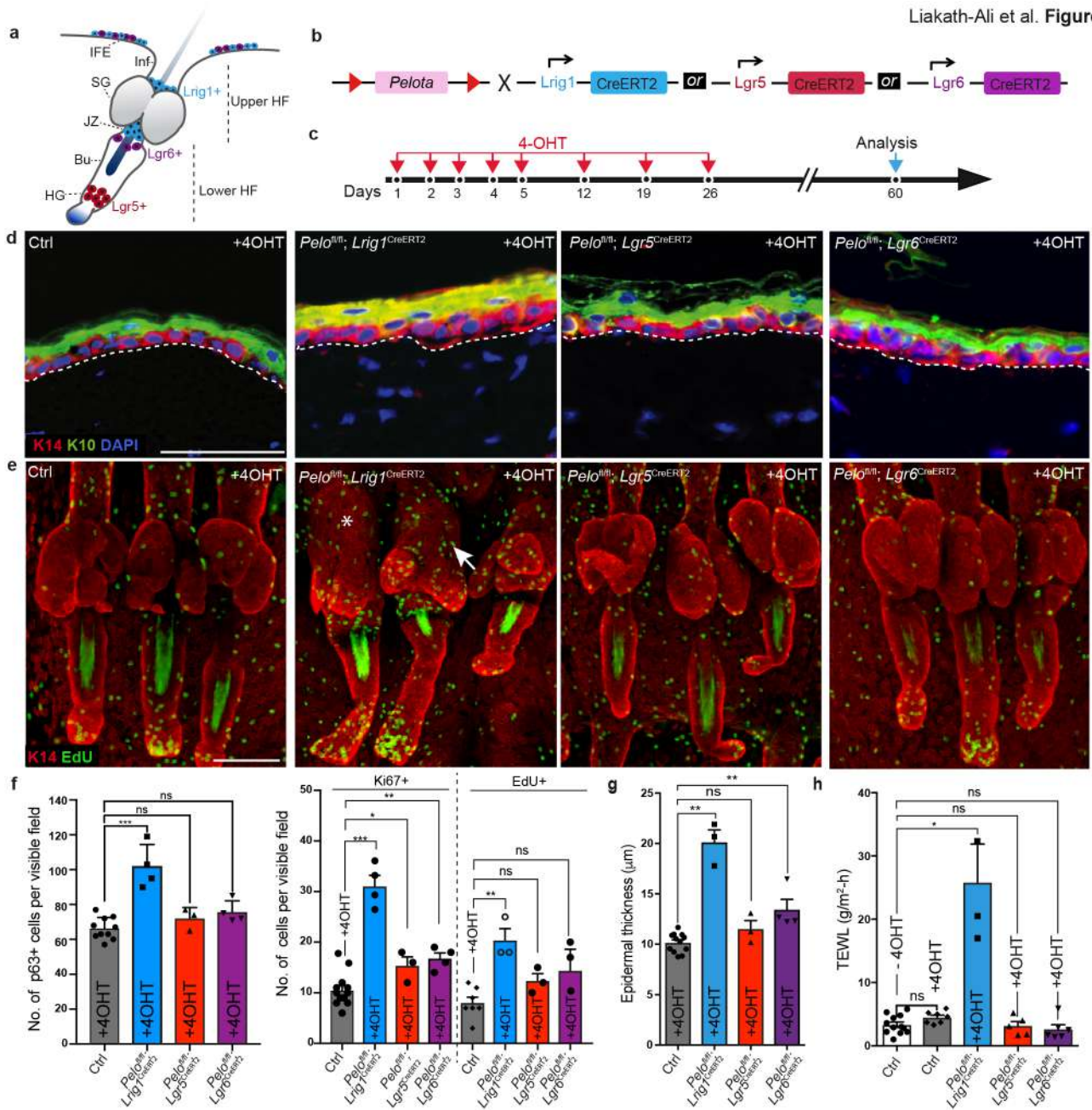


Fig. 2. *Lrig1*⁺ stem cells account for *Pelo* mutant epidermal phenotype (a-c) Schematics of *Lrig1*, *Lgr5* and *Lgr6* expression (a), breeding (b) and 4-OHT treatment (c). (d, e) Immunostaining of dorsal skin IFE sections (d) and tail wholemounts (e) with antibodies to the markers shown. (e) Asterisk: altered SG; arrow: altered JZ. (g-i) Quantification of proliferation (f), epidermal thickness (g) and TEWL (h). IFE, interfollicular epidermis; Inf, infundibulum; SG, sebaceous gland; JZ junctional zone; Bu, bulge; HG, hair germ. Scale bars 50 μ m (d, f); 100 μ m (e). Dashed lines: epidermal-dermal boundary. *** $p=0.0010$ (g, p63); *** $p=0.0005$; * $p=0.0330$, ** $p=0.0071$ (g, Ki67); ** $p=0.0083$ (g, EdU). ** $p=0.0044$, 0.0011 (h). * $p=0.0167$ (i), $n=3$ to 5 mice per group. n.s., non significant.

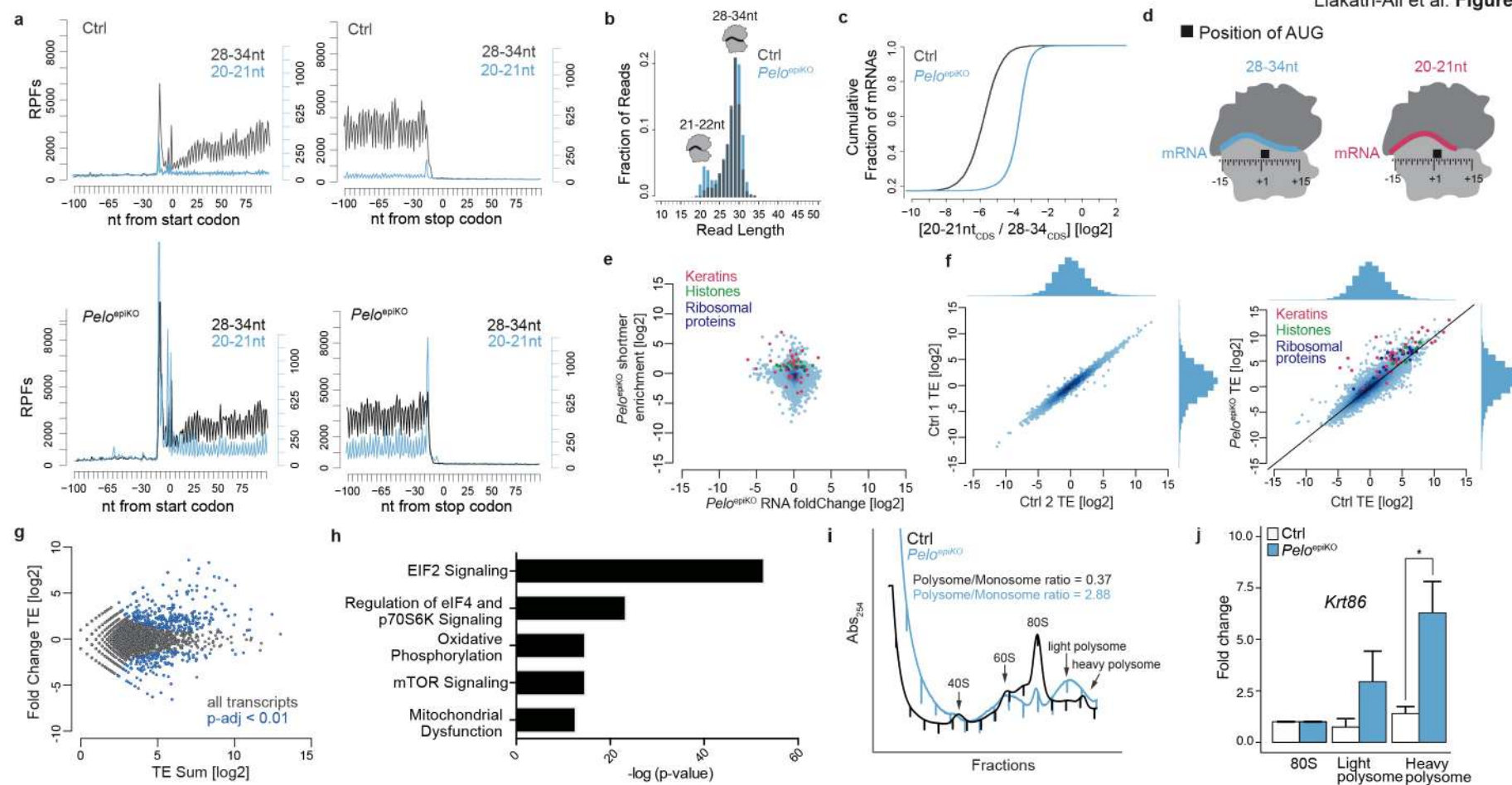


Fig. 3. Accumulation of short ribosome footprints and global translational changes in *Pelo* knockout epidermis (a) Metagene analysis of full length and short RPFs near the start (left) and stop (right) codons. (b) RPF read length distributions. (c) Empiric cumulative distribution plot of global enrichment of short 20-21nt relative to expected 28-34nt reads. (d) Designations of -15 peaks indicate positions of 5' end of RPF; corresponding P site occupancy shown. (e) Relative enrichment of short RPFs (y-axis) and change in RNA transcript levels (x-axis). (f) Replicate analysis of translational efficiency (TE). (g) MA plot showing observed and expected variance in TE measurements; p-adjusted <0.01, blue transcripts. (h) Canonical pathways linked to translation regulation in *Pelo*^{epiKO}. (i) Epidermal polysome profiling. (j) qRT-PCR shows significant increase in heavy polysome bound *Krt86* mRNA; $p=0.019$.

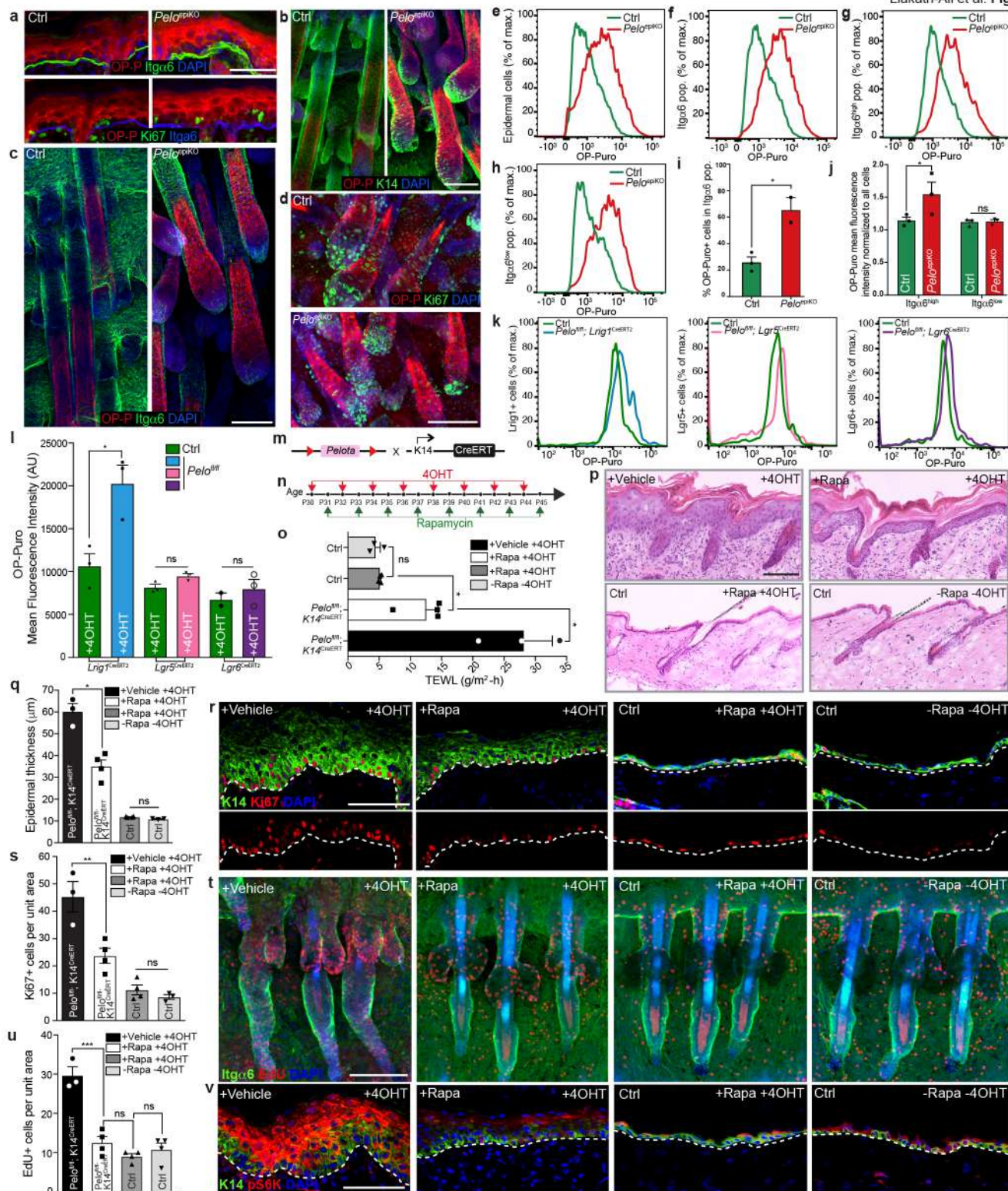


Fig. 4. Inhibition of mTOR pathway attenuates Pelo phenotype progression (a-d, r, t, v)

Immunolabelling for markers indicated. (s, u) Quantitation: $**p=0.0064$ (s); $***p=0.0006$ (u). (b-l) OP-Puro injected newborn (b-j) and adult (k, l) mice. (e-k) Representative flow histograms and (i, j, l) quantitation; $n=3$ mice per group. $*p=0.0406$ (i), 0.0357 (j), 0.0198 (l). (m-v) 4-OHT and rapamycin (Rapa) treatment. (o) TEWL; $*p=0.0145$. (p, q) H&E stained dorsal skin. $*p=0.0286$. Scale bars $50\ \mu\text{m}$ (a); $100\ \mu\text{m}$ (b-d; p, r, s, v), $n = 3-4$ mice per group.